A Unity Power Factor Buck Pre-Regulator with the Feedforward Control Technique

Fabiana Pöttker de Souza and Ivo Barbi
Federal University of Santa Catarina - Department of Electrical Engineering - Power Electronics Institute
P. O. BOX 5119 – 88040-970 – Florianópolis – SC - Brazil
Phone: 55-48-331.9204 – FAX: 55-48-234.5422 – E-mail: fabiana@inep.ufsc.br

***Abstract* - This paper presents a new technique to get unity power factor in a single-phase rectifier based on a Buck pre-regulator. The proposed feedforward control technique, allows the use of a small low frequency inductor with a high current ripple. Theoretical analysis, design procedure and experimental results of a 750W, 30kHz prototype are presented.**

I. Introduction

The Buck pre-regulator presented in Fig. 1 has some important characteristics such as the absence of inrush current, low DC output voltage, protection against short circuit, among others.

In discontinuous conduction mode [1], with a high frequency output inductor L_o, the input current is zero while the instantaneous value of the input voltage is smaller than the output voltage. The input current harmonic distortion is dependent on the ratio between the output voltage average value and the input voltage peak value. Fig. 2 shows the simulation results for an inductance L_o of 95μH. Depending on the design, the third and the fifth harmonic components may not be in compliance with the IEC 61000-3-2 standard [2]. Another disadvantage of the discontinuous conduction mode is that the peak and rms currents are very high, leading to high conduction losses in the switches.

On the other hand, in continuous conduction mode, with a low frequency output inductor designed in such a way that it behaves as a constant current source, the problem stated above no longer exists. However the inductor size and weight in this case is much bigger. The employed control technique is presented in Fig. 3. The output voltage is sensor and compared to a reference voltage. The resulting error is the input of an appropriate voltage controller. A sensor of the rectified input voltage multiplies the voltage controller output signal. The resulting modulation signal is compared with the saw-tooth signal, generating the drive signal to the switch S_b. In Fig. 4 it is presented the simulation results employing this control strategy, for an inductance L_o of 1H. As it can be noticed the input current is practically sinusoidal and a high power factor is achieved.

In order to optimize the size and weight, the inductance L_o may be decreased, so it no longer behaves as a constant current source. Although, increasing the output inductor current ripple distorts the input current, with a significant third harmonic component, as shown in the simulation results of Fig. 5, for an inductance L_o of 15mH.

Reference [3] proposes a control technique to eliminate the input current distortion due to the output inductor current ripple. The difference between this technique and the one presented in Fig. 3 is that the modulation signal is compared to a saw-tooth whose peak value is proportional to the current i_{Lo}. The current i_{Lo} is detected and fed into an integrator circuit, which is reset at a constant interval and its output is the saw-tooth whose peak value is proportional to the inductor current. The feedforward control technique presented in this work also eliminates the input current distortion due to the output inductor current ripple, however, on a different way. The difference between the proposed technique and the one presented by [3] is that the information about the output inductor current is on the modulation signal instead of being in the saw-tooth signal. The authors believe that this is an easier way to implement this technique.

With a technique to eliminate the input current distortion due to the output inductor current ripple, the current ripple could be increased to optimize the inductor size and weight. However, there is a limit. This limit and another important issues are presented in the theoretical analysis of Section III.

II. Control Strategy

The buck pre-regulator with the feedforward control technique is presented in Fig. 6. The output voltage is sensor and compared to a reference voltage. The resulting error is the input of an appropriate voltage controller. The voltage controller output signal is multiplied by a sensor of the rectified input voltage and divided by a sensor of the output inductor current. The resulting modulation signal is compared with the saw-tooth signal, generating the drive signal to the switch S_b.

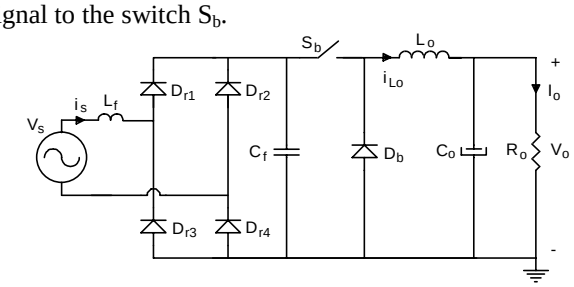

Fig. 1. The Buck pre-regulator.

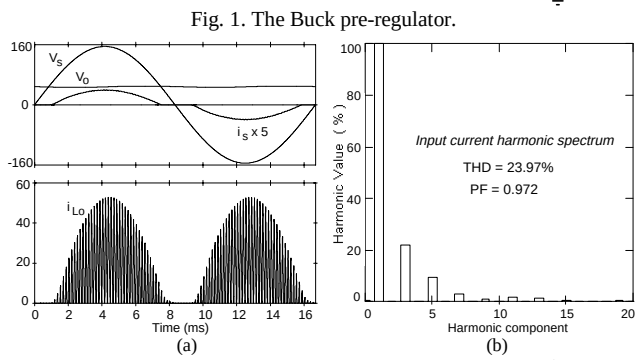

Fig. 2. Discontinuous conduction mode simulation results for an inductance L_o of 95μH.

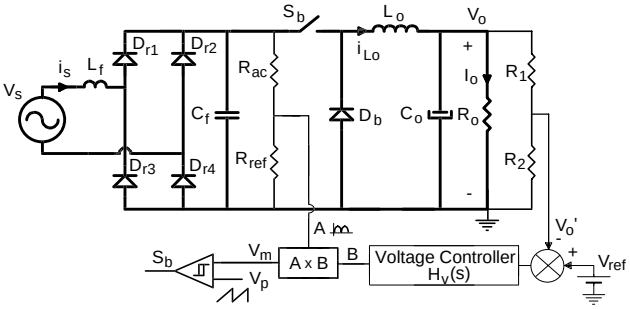

Fig. 3. The Buck pre-regulator control diagram for the continuous conduction mode.

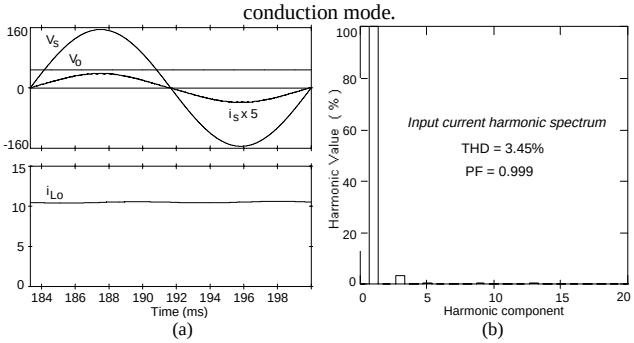

Fig. 4. Continuous conduction mode simulation results for an inductance L_o of 1H.

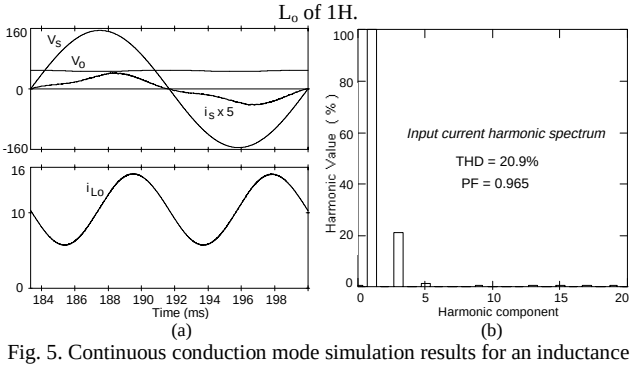

Fig. 5. Continuous conduction mode simulation results for an inductance L_o of 15mH.

In Fig. 7(a) it is presented the output inductor current and the resulting modulation signal. Thanks to the feedforward control technique the modulation signal presents a distortion that eliminates the input current distortion due to the output inductor current ripple. In Fig. 7(b) it is presented the saw-tooth signal being compared to the modulation signal and the resulting drive signal to the switch S_b.

In Fig. 8 it is presented the simulation results employing the proposed control strategy, for the same specifications of Fig. 5. The third harmonic was almost eliminated resulting in a high power factor.

Without the feedforward control technique there is no information about the output inductor current, so the modulation signal, obtained by the multiplication of "A" and "B", results in a sinusoidal signal.

III. Theoretical Analysis

A. Output Inductor Current Ripple Limit

In a Buck converter the output current is bigger than the input current. The limit for the output inductor current ripple is the one that guarantees that the output inductor current equals the input current in one point only, as shown in Fig. 9. Otherwise the input current will be distorted, as shown in Fig. 10. Equation (1) and (2) define the input current and output inductor current, respectively.

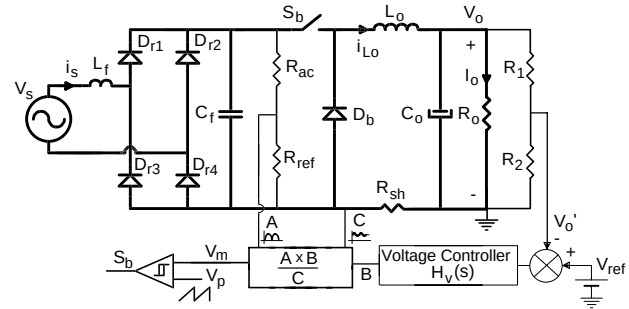

Fig. 6. The Buck pre-regulator control diagram with the proposed feedforward control technique.

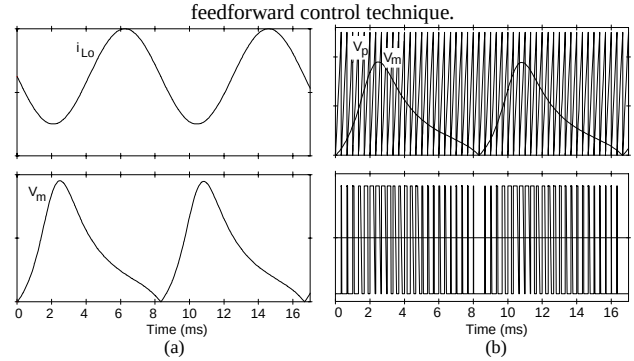

Fig. 7. Simulation results of the proposed feedforward control technique for a low switching frequency.

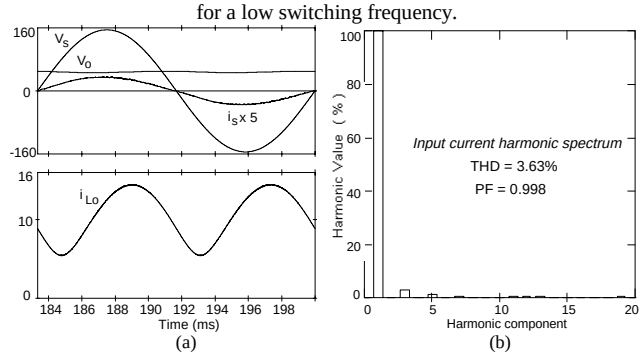

Fig. 8. Simulation results of the proposed feedforward control technique for an inductance L_o of 15mH.

$$i_s(\theta) = i_{s_{peak}} \sin(\theta) \tag{1}$$

$$i_{Lo}(\theta) = I_o - \frac{\Delta I_o}{2} \sin(2\theta) \tag{2}$$

In order to find out the maximum output inductor current ripple, (1) and (2) are made equal, resulting in (3).

$$\overline{\Delta I_o} = \frac{\Delta I_o}{I_o} = 2\left(1 - M_i \sin(\theta)\right) / \sin(2\theta) \tag{3}$$

Where: $M_i \rightarrow$ modulation index: $M_i = i_{s_{peak}} / I_o$,

$\overline{\Delta I_o} \rightarrow$ parameterized current ripple.

In order to obtain the angle θ_t where the currents touch each other in one point, (3) is derived and made equal to zero, as shown in (4). Solving (4) algebraically the angle θ_t is obtained as a function of the modulation index, as shown in Fig. 11. The currents will touch in one point always between 45° and 90°. Substituting the angle θ_t in (3) the maximum parameterized current ripple is obtained as a function of the modulation index, as shown in Fig 12.

$$\frac{d\overline{\Delta I_o}}{d\theta} = \frac{2\left(-\sin(2\theta) M_i \cos(\theta) - 2\left(1 - M_i \operatorname{sen}(\theta)\cos(2\theta)\right)\right)}{\left[\sin(2\theta)\right]^2} = 0 \tag{4}$$

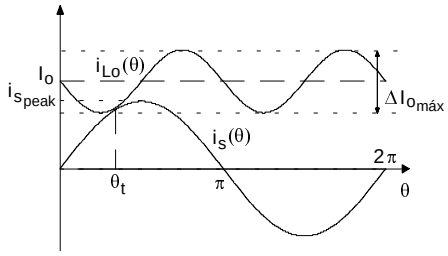

Fig. 9. Output inductor current ripple limit.

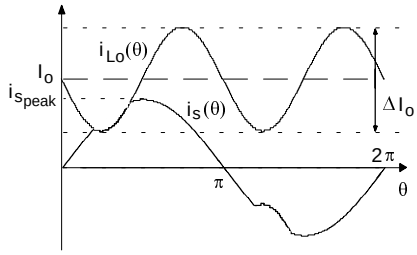

Fig. 10. Beyond the output inductor current ripple limit.

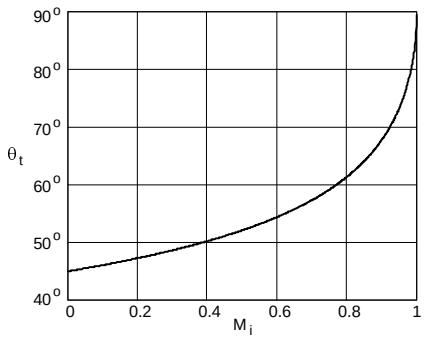

Fig. 11. Angle θ_t as a function of the modulation index.

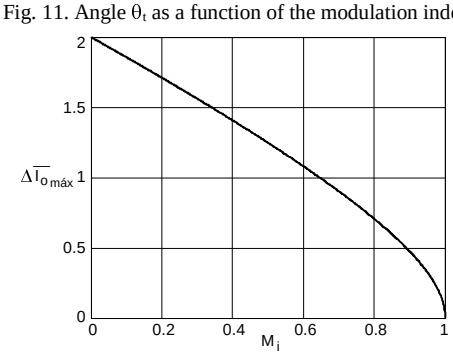

Fig. 12. Maximum parameterized current ripple as a function of the modulation index.

B. Output Characteristics

The average output voltage without the feedforward control technique is represented by (5), and with the feedforward control technique is represented by (6). The output characteristics are presented in Fig. 13 and 14. As can be noticed, with the feedforward control technique the average output voltage is dependent on the output current, and without the feedforward control technique the average output voltage is independent of the output current.

$$\overline{V_{o\,avg}} = \frac{V_{o\,avg}}{V_{s\,peak}} = \frac{M_i}{2} \tag{5}$$

$$\overline{V_{o\,avg}} = \frac{V_{o\,avg}}{V_{s\,peak}} = \frac{\overline{V_m}}{2\,\overline{I_o}} \tag{6}$$

Where: $\overline{V_m} = V_m / V_{m\,max}$, $\overline{I_o} = R_{sh}\, I_o / V_{m\,max}$.

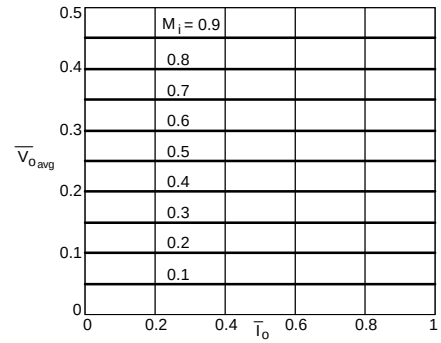

Fig. 13. Output characteristics without the feedforward control technique.

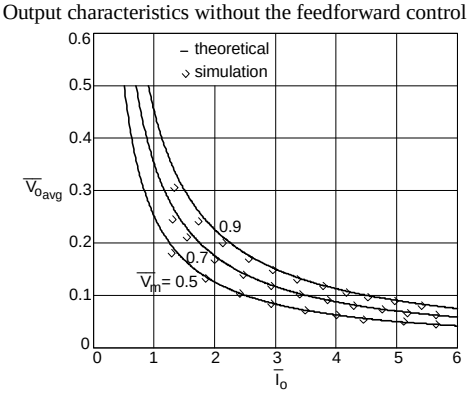

Fig. 14. Output characteristics with the feedforward control technique.

Equation (7) presents the transfer function of the output voltage versus the output inductor current. The voltage controller, presented in Fig. 15, is a proportional integral one, in order to ensure a null static error. Its transfer function is defined by (8).

$$G_v(s) = \frac{V_o(s)}{i_{Lo}(s)} = \frac{R_o}{(1 + s\,C_o\,R_o)} \tag{7}$$

$$H_v(s) = \frac{V_o'(s)}{V_c(s)} = \frac{-(1 + s\,R_{v2}\,C_{v1})}{s\,C_{v1}\,R_{v1}} \tag{8}$$

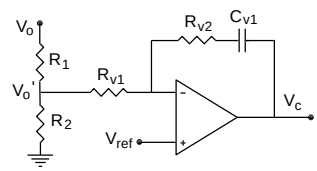

Fig. 15. Voltage controller.

IV. Design Methodology and Example

A simplified design procedure and example is described in this section, according to the analysis presented in Section III. The specifications are as follows:

V_{speak} = 311V f_{line} = 60Hz P_{onom}=1.5kW f_s = 30kHz I_{onom}=25A P_{omin}=0.5 P_{onom}=750W I_{omin}=12.5A V_o=60V ΔV_o=10%V_o=6V

The input current for nominal and minimum power and the modulation index are calculated as follows:

$$i_{s\,peak_{nom}} = \frac{2\,P_{o\,nom}}{V_{s\,peak}} = \frac{2 \times 1500}{311} = 9.65\text{A}$$

$$i_{s\,peak_{min}} = \frac{2\,P_{o\,min}}{V_{s\,peak}} = \frac{2 \times 750}{311} = 4.82\text{A}$$

$$M_i = \frac{i_{s\,peak_{nom}}}{I_{o\,nom}} = \frac{i_{s\,peak_{min}}}{I_{o\,min}} = \frac{9.65}{25} = 0.386$$

The maximum parameterized current ripple is calculated as shown bellow.

$$\frac{d\Delta\overline{I_o}}{d\theta} = \frac{d}{d\theta}\left(2\frac{1-M_i\sin(\theta)}{\sin(2\theta)}\right) = 0 \Rightarrow \theta_t = 50^o$$

$$\Delta\overline{I_o}_{max} = 2\left(\frac{1-M_i\sin(\theta_t)}{\sin(2\theta_t)}\right) = 2\times\left(\frac{1-0.386\times\sin(50^o)}{\sin(2\times 50^o)}\right) = 143\%$$

The maximum parameterized current ripple shall occur in the minimum power, so the current ripple is calculated.

$$\Delta I_o = \Delta\overline{I_o}_{max}\times I_{o_{min}} = 1.43\times 12.5 = 17.9A$$

Once the output inductor current ripple and the output voltage ripple are defined, the inductance L_o and capacitance C_o are calculated.

$$L_o = \frac{P_{o\,nom}}{2\pi f_{line} I_o \Delta I_o} = \frac{1500}{2\times\pi\times 60\times 25\times 17.9} = 8.9mH$$

$$C_o = \frac{\Delta I_o}{4\pi f_{line}\Delta V_o} = \frac{17.8}{4\times\pi\times 60\times 6} = 3.93mF \Rightarrow 4.3mF$$

The capacitor C_o rms current is calculated as follows:

$$i_{Co_{rms}} = \frac{\Delta I_o}{2\sqrt{2}} = \frac{17,9}{2\sqrt{2}} = 6.33A$$

The high frequency input filter (L_f and C_f) is calculated according to the following procedure.

$$f_c = f_s/10 = 3kHz \Rightarrow w_c = 18850\,rad/s$$

$$\zeta = 1.0$$

$$R_{eq} = \frac{V_{s\,peak}}{i_{s\,peak_{nom}}} = \frac{311}{9.65} = 32.24\Omega$$

$$C_f = \frac{1}{R_{eq}\,2\zeta\,w_c} = \frac{1}{32.24\times 2\times 1\times 18850} \cong 0.8\mu F$$

$$L_f = \frac{1}{w_c^{\,2}\,C_f} = \frac{1}{18850^2\times 0.8\mu} \cong 3.5mH$$

Adjusting the filter by simulation: $\begin{cases} C_f = 2\mu F \\ L_f = 1.4mH \end{cases}$

The $G_v(s)$ transfer function is calculated as shown bellow.

$$G_v(s) = \frac{R_{o\,nom}}{1+s\,C_o\,R_{o\,nom}} = \frac{2.4}{1+s\,126.26}$$

The pole occurs approximately in 126rad/sec. The voltage compensator zero shall occur near the pole so that they cancel each other. Choosing $R_{v1} = 67k\Omega$ and $R_{v2} = 33k\Omega$, C_{v1} is calculated.

$$C_{v1} = \frac{1}{126\times 33\times 10^3} = 240nF \Rightarrow C_{v1} = 220nF$$

The output voltage is sensored with a gain of 0.05.

$$H_v(s) = k_{Vo}\frac{1+s\,R_{v2}\,C_{v1}}{s\,R_{v1}\,C_{v1}} = 50\times 10^{-3}\times\frac{1+s\,137.74}{s\,0.01474}$$

The Bode diagram of $G_v(s)$, $H_v(s)$ and the open loop transfer function are presented in Fig. 16. The crossover frequency is about 1.5Hz.

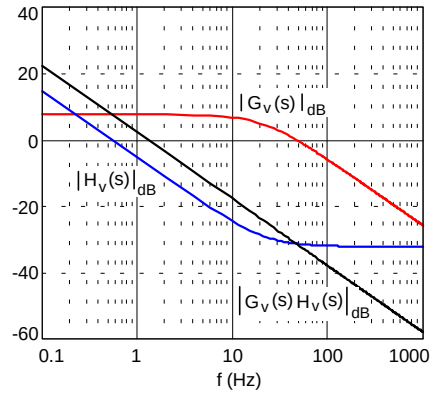

Fig. 16. Bode diagram of $G_V(s)$, $H_V(s)$ and $G_V(s)\,H_V(s)$.

V. Experimental Results

In order to verify the principle of operation and the control strategy the designed prototype was built. The inductance L_o was designed to have a current ripple a little smaller than the output inductor current ripple limit. In order to implement the feedforward, multiplying A and B and dividing by C, two dedicated integrated circuit UC3854 [4] were used, as shown in Fig. 17.

In Fig. 18 it is presented the complete diagram of the implemented prototype. A passive non-dissipative snubber [5] is used, as shown in the shadow areas of Fig. 18. The inductor L_s is responsible for the "lagging effect" in the reverse recovery of diode D_b, reducing the turn on losses of switch S_b. The parameter and power component specifications are as follows:

$V_s = 220V_{rms}$ $f_{line} = 60Hz$ $V_o = 60V$ P_o=750W

C_o = 2 x (4.3mF/75V) C_f = 2uF/280V (polypropylen)

L_f = 1.4mH – 42 turns (2x14AWG) on 2.8cm FeSi core (gap = 0.28mm)

L_s = 3.4μ/H – 5 turns (15 x 19AWG) on EE30/7 core

C_s = 100nF S_b: IRG4PC50W D_b: APT30D100BN

L_o = 8.9mH – 63 turns (5 x 12AWG) on 6cm FeSi core (gap = 0.24cm)

In Fig. 19 it is presented the input voltage and current and the input current harmonic spectrum, with the feedforward control technique. The total harmonic distortion, considering up to the 60th component, is 5.39% and the current phase displacement is 1.72° resulting in a power factor of 0.998. The input voltage presented a total harmonic distortion of 2.87%. In Fig. 20 it is shown the output inductor current and the input current. As expected, the output inductor current ripple is a little smaller than the output inductor current ripple limit.

The input voltage and current and the input current harmonic spectrum, without the feedforward control technique, are shown in Fig. 21. The power factor decreased to 0.948 and the third harmonic is significant. In Fig. 20 (c) and 21 (b) it is presented the modulation signal with and without the feedforward control strategy. It can be noticed that without the feedforward control technique the modulation signal is sinusoidal, and with the

feedforward control technique there is a distortion due to the output inductor current ripple, which eliminates the input current distortion.

In Fig. 22 it is presented the input voltage and current and the input current harmonic spectrum, with the feedforward control technique a little beyond the output inductor current ripple limit. The power factor decreased to 0.994. The design shall be made to reach the output inductor current ripple limit on a “critical power”. Therefore, for a power smaller than the critical, the input current will be distorted as shown in Fig. 21, and for a power bigger than the critical, the power factor will be close to unity.

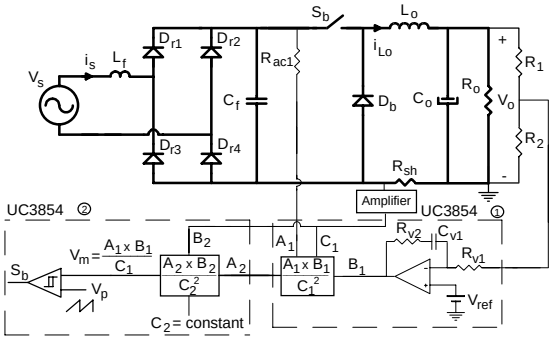

Fig. 17. Block diagram of the implemented prototype

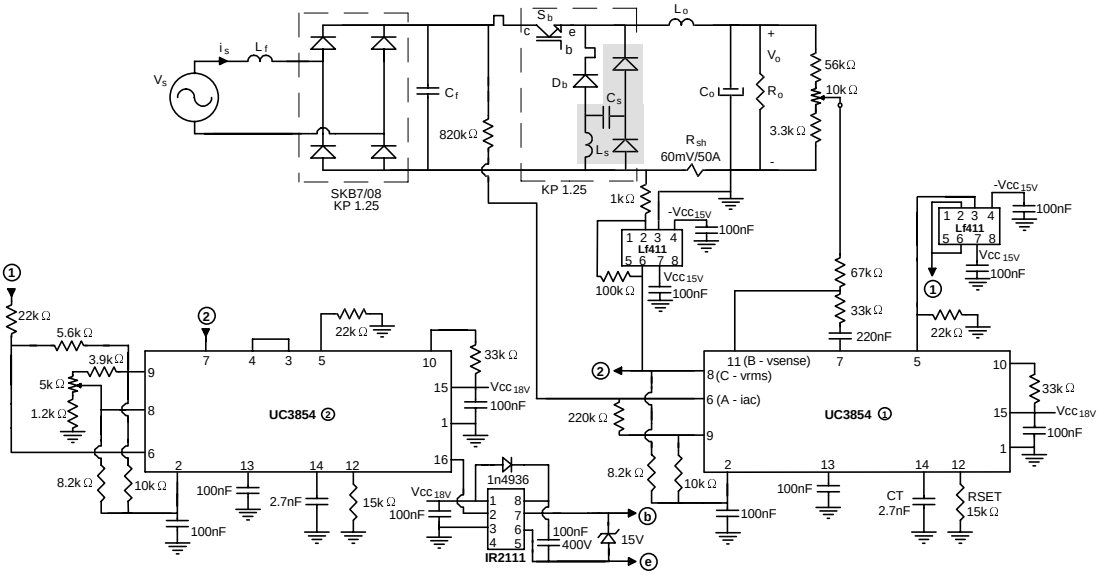

Fig. 18. Complete diagram of the implemented prototype.

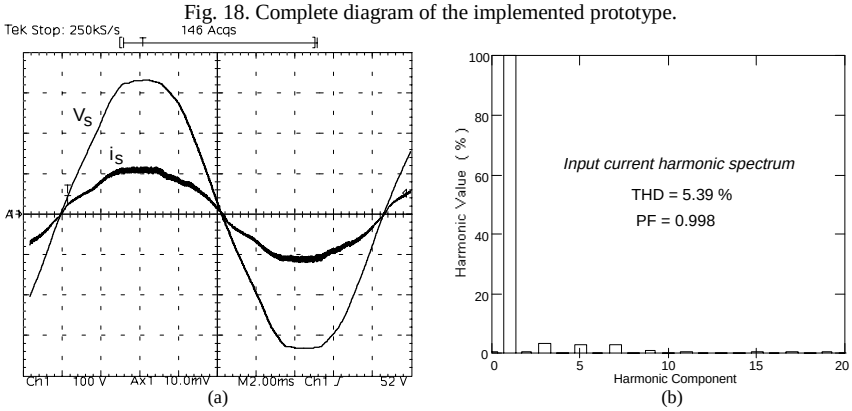

(a) (b)

Fig. 19. Experimental results with the feedforward control technique: (a) Input voltage (100V/div.) and input current (5A/div.), (b) input current harmonic spectrum.

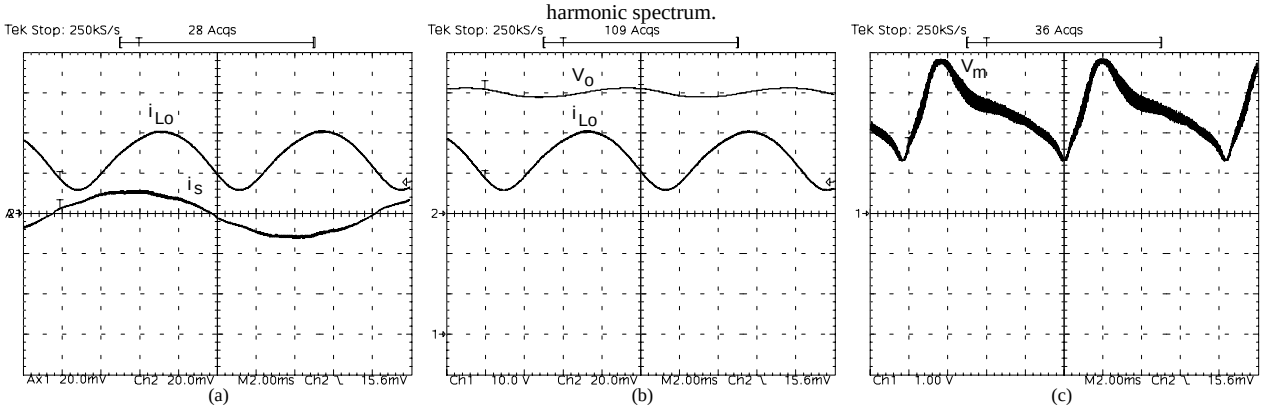

(a) (b) (c)

Fig. 20. Experimental results with the feedforward control technique: (a) Output inductor current (10A/div.) and input current (10A/div.), (b) output voltage (10V/div.) and output inductor current (10A/div.), (c) modulation signal (1V/div.).

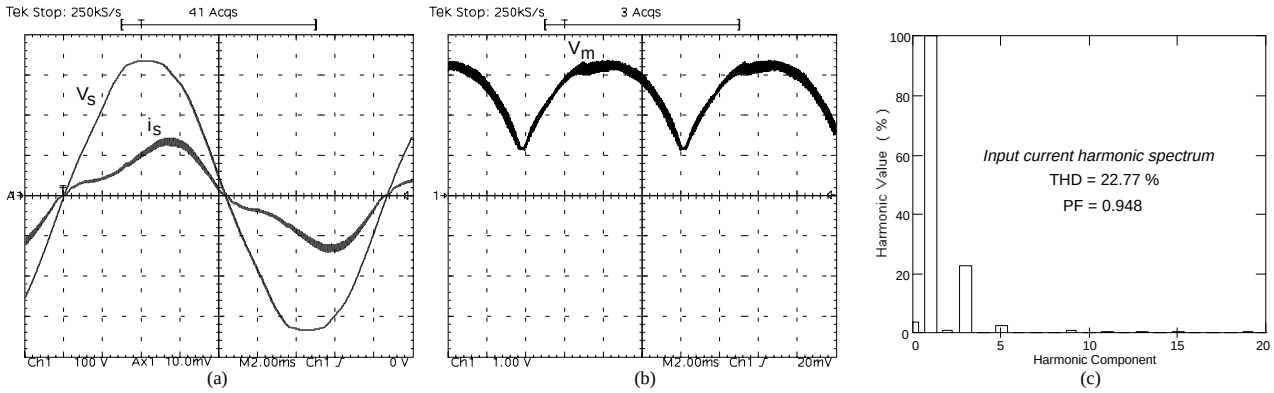

Fig. 21. Experimental results without the feedforwad control technique: (a) Input voltage (100V/div.) and input current (5A/div.), (b) modulation signal (1V/div.), (c) input current harmonic spectrum.

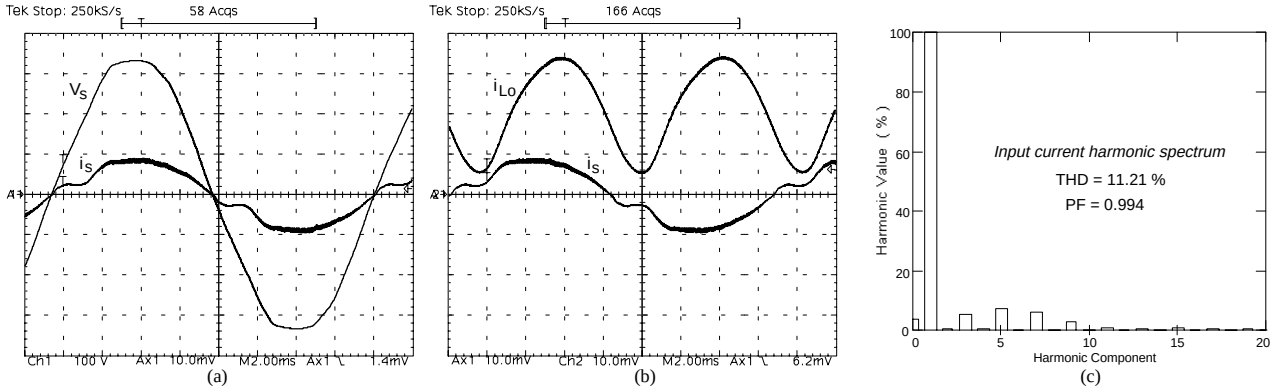

Fig. 22. Experimental results with the feedforwad control technique beyond the output inductor current ripple limit: (a) Input voltage (100V/div.) and input current (5A/div.), (b) output inductor current (5A/div.) and input current (5A/div.), (c) input current harmonic spectrum.

VI. Conclusion

In this paper it is presented and analyzed a control strategy to reduce the size, weigh and cost of a Buck based unity power factor single-phase rectifier, operating in continuous conduction mode.

From these studies, the following conclusions are drawn:

- The power factor is independent on the ratio between the output voltage average value and the input voltage peak value.
- Despite the utilization of a “small” filter inductor and a high 120Hz current ripple, the power factor is close to unity.
- The practical implementation is easy, with the utilization of a well-known dedicated integrated circuit (UC3854).

VII. References

[1] H. Endo, T. Yamashita, T. Sigiura, “A high-power-factor Buck converter”, IEEE PESC Records, 1992, pp. 1071-1076.

[2] IEC, IEC 61000-3-2 Standard, International Eletrotechnic Commission, 1998, Geneve, Switzerland.

[3] K. Hirachi, T. Iwade, K. Shibayama, “A specific control implementation on Buck-type active power filtering converters”, IEEE INTELEC Records, 1995, pp. 444-449.

[4] C. S. Silva, “Power factor correction with UC3854”, Unitrode Application Note U-125, 1990, Merrimack, NH, EUA.

[5] D. Tardiff, T. H. Barton, “A summary of resonant snubber circuits for transistors and GTOs”, IEEE IAS Records, 1989, pp. 1176-1180.